

Supplementary Information

A highly stabilized nickel-rich cathode material by nanoscale epitaxy control for high-energy lithium-ion batteries

Junhyeok Kim,^a Hyunsoo Ma,^a Hyungyeon Cha,^a Hyomyung Lee,^a Jaekyung Sung,^a Minho
Seo,^a Pilgun Oh,^{a,*} Minjoon Park^{†,a,*}, and Jaephil Cho^{a,*}

^aDepartment of Energy Engineering, School of Energy and Chemical Engineering, Ulsan
National Institute of Science and Technology (UNIST), 50, UNIST-gil, Ulsan 44919, Republic
of Korea

[†]Present Address: Harvard John A. Paulson School of Engineering and Applied Science, 29
Oxford Street, Cambridge, MA 02138, USA

*e-mail: smartoh@unist.ac.kr, pmjdotcom@seas.harvard.edu, jpcho@unist.ac.kr

MATERIALS AND METHODS

Preparation of the NCM and NS-NCM For the synthesis of the $\text{LiNi}_{0.8}\text{Co}_{0.1}\text{Mn}_{0.1}\text{O}_2$ (NCM) cathode, we employed conventional co-precipitation method. The transition metal solution was prepared by using nickel (II) sulfate hexahydrate ($\text{NiSO}_4 \cdot 6\text{H}_2\text{O}$), cobalt (II) sulfate heptahydrate ($\text{CoSO}_4 \cdot 7\text{H}_2\text{O}$), and manganese sulfate pentahydrate ($\text{MnSO}_4 \cdot 6\text{H}_2\text{O}$) with a molar ratio of 0.8:0.1:0.1. Also, we prepared the sodium hydroxide (NaOH) and ammonia (NH_4OH) solution with a concentration of 4.0 M and 0.4 M, respectively. The transition metal, sodium hydroxide, and ammonia solution were fed into 4 L batch co-precipitation reactor with feeding rates of 300, 300, and 30 ml h^{-1} , respectively. The temperature of the co-precipitation reactor was maintained to 50°C . The reaction time was set as 18 h for synthesizing $\text{Ni}_{0.8}\text{Co}_{0.1}\text{Mn}_{0.1}(\text{OH})_2$. This cathode precursor was mixed with lithium hydroxide ($\text{LiOH} \cdot \text{H}_2\text{O}$, molar ratio of 1:1.03), and annealed the mixture at 820°C for 15 h. For the stabilizer precursor, the stoichiometric amount of the cobalt acetate ($\text{Co}(\text{CH}_3\text{COO})_2 \cdot 4\text{H}_2\text{O}$, 10 g) was dissolved in the de-ionized water (50 ml), and the sodium hydroxide (NaOH, 3.3 g) was added into the solution, resulting in the precipitation reaction between Co^{2+} and OH^- . The precipitated solution was continuously stirred under 350 r.p.m for 30 min. The solution was filtered and dried at 120°C for 1h. For the formation of the nanostructured stabilizer, the prepared precursor (4 g) was physically mixed with the NCM powder (100 g) by using planetary centrifugal mixer with a rotating speed of 1,500 r.p.m. for 10 min, then annealed at 750°C for 4 h.

Material characterization: The amount of residual lithium compounds was measured by a potentiometric titrator (888 Titrand, Metrohm). For measuring these compounds, the active materials (~10 g) were stirred in de-ionized water (~100 ml) for 15 min, then the solution was filtered. The filtered solution was titrated by using 0.1 M hydrochloric acid (HCl). The X-ray

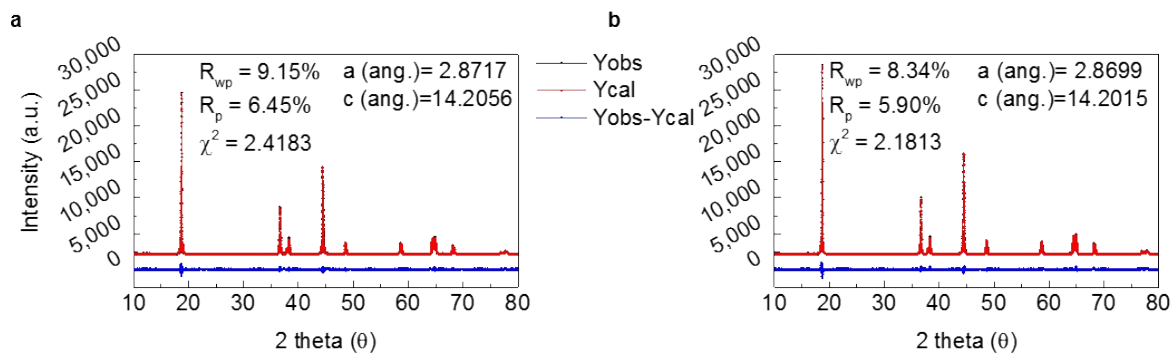
diffraction (XRD) patterns were obtained by using Rigaku D/MAX 2500 V/PC X-ray diffractometer with Cu-K α radiation. The morphology of the cathode powder was analyzed by scanning electron microscopy (SEM, Verios 460, FEI). Cross-sectional images of the cathode particles were obtained by using focused ion beam (FIB, Helios Nano Lab450, FEI). For analyzing surface microstructure of the cathode and anode particles, the cross-sectioned samples were thinned by Ar ion milling system (Model 1040 Nanomill, Fischione). After thinning the samples, the structural and chemical analysis was performed using a high resolution transmission electron microscope (HR-TEM, ARM300, JEOL) operating at 160 kV. The energy dispersive X-ray spectroscopy (EDX) and electron energy loss spectroscopy (EELS) results were attained using the same HR-TEM. Surface chemistry was analyzed using X-ray photon spectroscopy (XPS, Thermo Scientific K α spectrometer). To analyze the cycled electrode, the cycled full-cells were disassembled in the dry room with humidity < 0.1% to avoid contact with the moisture. After disassembling the cells, the cycled electrodes were gently washed with dimethyl carbonate (DMC) to eliminate residual electrolyte salt and by-products, then were analyzed.

Electrochemical characterization: All half cells were assembled using 2032R type coin cell. The positive electrode was prepared by mixing the cathode powder (96wt.%), Super-P (2wt.%), and poly(vinylidene fluoride) binder (2wt.%) in N-methyl-2-pyrrolidinon. The cathode loading level and electrode density were $\sim 12 \text{ mg cm}^{-2}$ and $\sim 3.0 \text{ g cm}^{-3}$, respectively. The electrolyte for the half-cell evaluation was 1 M LiPF $_6$ with ethylene carbonate, ethyl methyl carbonate (10:20vol.%) (Panax Etec.). The separators for the half-cell evaluation was microporous polypropylene (PP)/ polyethylene (PE)/ PP composite (Celgard) with a thickness of 25 μm . All half-cells were assembled in Ar-filled glove box. All cathode half-cells were evaluated with constant current (CC) – constant voltage (CV) mode between 3.0 and 4.3 V. The first charge

and discharge cycle test was performed at charge and discharge C-rate of 0.1C. The cycle performance was evaluated at charge and discharge C-rate of 0.5 and 1C, respectively. The negative electrode was fabricated by mixing the conventional graphite (96wt.%), Super-P (1wt.%), carboxymethyl cellulose (CMC, 1.5wt.%), and styrene butadiene rubber (SBR, 1.5wt.%). The anode loading level and electrode density were $\sim 7 \text{ mg cm}^{-2}$ and $\sim 1.6 \text{ g cm}^{-3}$, respectively. The electrolyte was 1.3 M LiPF_6 in ethylene carbonate, ethyl methyl carbonate, and diethyl carbonate (30:50:20 vol.%) with 10% fluoroethylene carbonate, 0.5% vinylene carbonate, and 0.2% lithium tetrafluoroborate. All anode half-cells were evaluated with CC – CV mode between 0.005 and 1.5 V. The first charge and discharge cycle test were performed at charge and discharge C-rate of 0.1C. The room temperature cycle test was performed at charge and discharge C-rate of 1C. For the full-cell design, we set the negative and positive electrode (N/P) ratio to ~ 1.05 . The parameters for positive electrode in full-cell such as electrode composition, loading level, and electrode density were same as the that for cathode half-cell. The parameters for negative electrode in the full-cell were also same as that for anode half-cell. The electrolyte was 1.05 M LiPF_6 in ethylene carbonate, ethyl methyl carbonate, and dimethyl ethylene carbonate (30:60:10vol.%) with 1wt.% vinylene carbonate and 0.5 wt.% 1,3-propane sultone. All full-cells were assembled in a pouch type cell and were evaluated with CC – CV mode between 2.8 and 4.2 V. First charge and discharge cycle test were performed with charge and discharge C-rate of 0.1 C. We charged the full-cells to 3.6 V during first charging process to eliminate the generated gaseous product (degassing process) in the full-cell. The cycle performance at 25°C and 45°C was evaluated at charge and discharge C-rate of 1C.

Table S1 | Outline of a variety of cobalt containing surface coating process for LIBs cathode materials with cobalt precursor sources and synthetic methods.

Cathode	Cobalt precursor	Synthetic method
This work	Cobalt hydroxide	Dry powder mixing
LiCoO ₂ coated LiNi _{0.6} Co _{0.2} Mn _{0.2} O ₂ (ref. 1)	Cobalt acetate	Sol-gel method
Li _x CoO ₂ coated LiNi _{0.8} Co _{0.15} Al _{0.05} O ₂ (ref. 2)	Cobalt acetate	Sol-gel method
Co ₃ O ₄ coated LiNi _{0.8} Co _{0.15} Al _{0.05} O ₂ (ref. 3)	Cobalt nitrate	Sol-gel method
Li _x CoPO ₄ coated LiNi _{0.8} Co _{0.16} Al _{0.04} O ₂ (ref. 4)	Cobalt nitrate	Sol-gel method
Co gradient incorporated LiMn ₂ O ₄ (ref. 5)	Cobalt acetate	Sol-gel method
LiCoO ₂ coated LiMn ₂ O ₄ (ref. 6)	Cobalt nitrate	Sol-gel method
LiCoO ₂ coated LiMn _{0.9} Co _{0.1} O ₂ (ref. 7)	Cobalt acetate	Sol-gel method
Co ₃ O ₄ coated 0.4Li _{4/3} Mn _{2/3} O ₂ 0.6LiNi _{1/3} Co _{1/3} Mn _{1/3} O ₂ (ref. 8)	Cobalt acetate	Hydrothermal method



	x	y	Z	Occupancy
Li (Li)	0	0	0.5	0.973
Ni (Ni)	0	0	0	0.773
Co (Co)	0	0	0	0.1
Mn (Mn)	0	0	0	0.1
O (O)	0	0	0.257	1
Li (Ni)	0	0	0	0.027
Ni (Li)	0	0	0.5	0.027

	x	y	Z	Occupancy
Li (Li)	0	0	0.5	0.98
Ni (Ni)	0	0	0	0.78
Co (Co)	0	0	0	0.1
Mn (Mn)	0	0	0	0.1
O (O)	0	0	0.257	1
Li (Ni)	0	0	0	0.02
Ni (Li)	0	0	0.5	0.02

Figure S1. Powder X-ray diffraction (XRD) patterns of the (a) NCM and (b) NS-NCM with the rietveld refinement results.

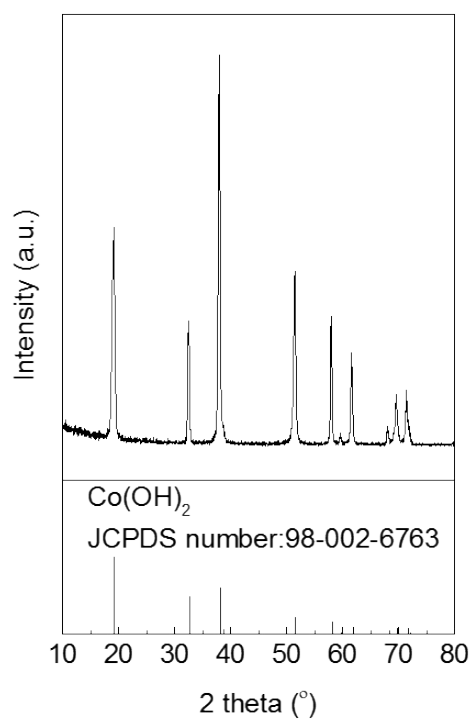


Figure S2. Powder XRD pattern of the stabilizer precursor.

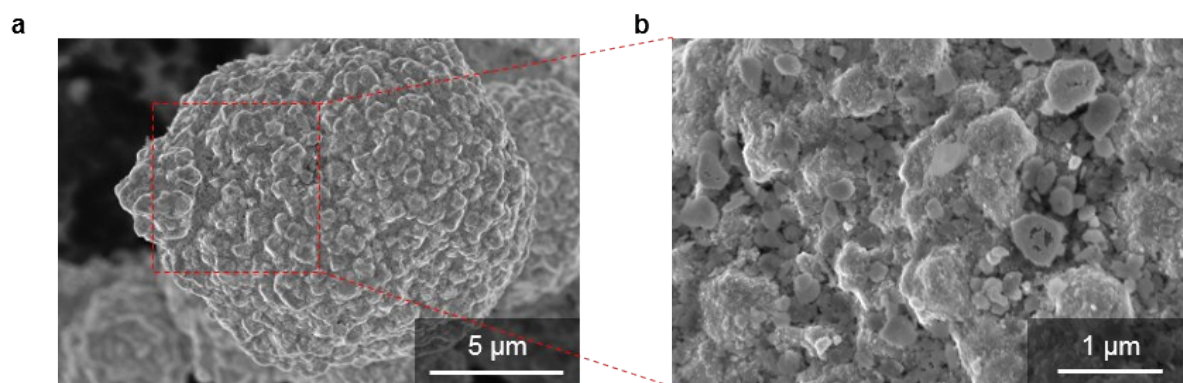


Figure S3. (a) A scanning electron microscopy (SEM) image of the mixture consisting of the NCM and stabilizer precursor. (b) A magnified SEM image from red box in (a).

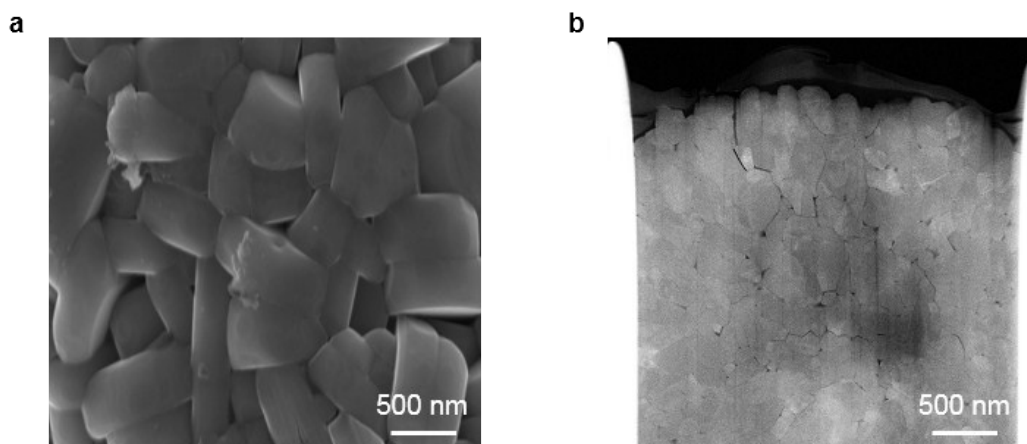


Figure S4. (a) Scanning electron microscopy (SEM) image of the NCM. (b) Cross-sectional SEM image of the NCM.

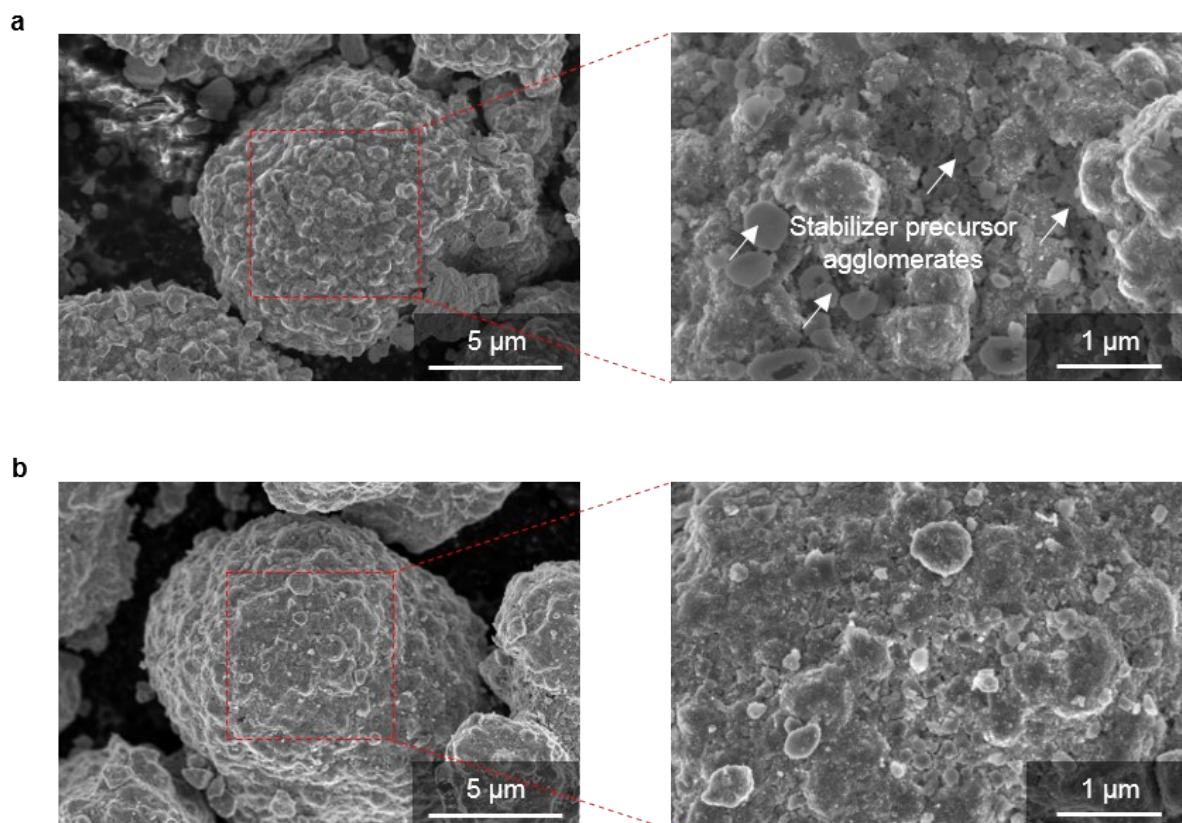


Figure S5. (a) Scanning electron microscopy (SEM) images of the mixture of the NCM and stabilizer precursor after annealing at 150°C. (b) Scanning electron microscopy (SEM) images

of the mixture of the NCM and stabilizer precursor after annealing at 200°C.

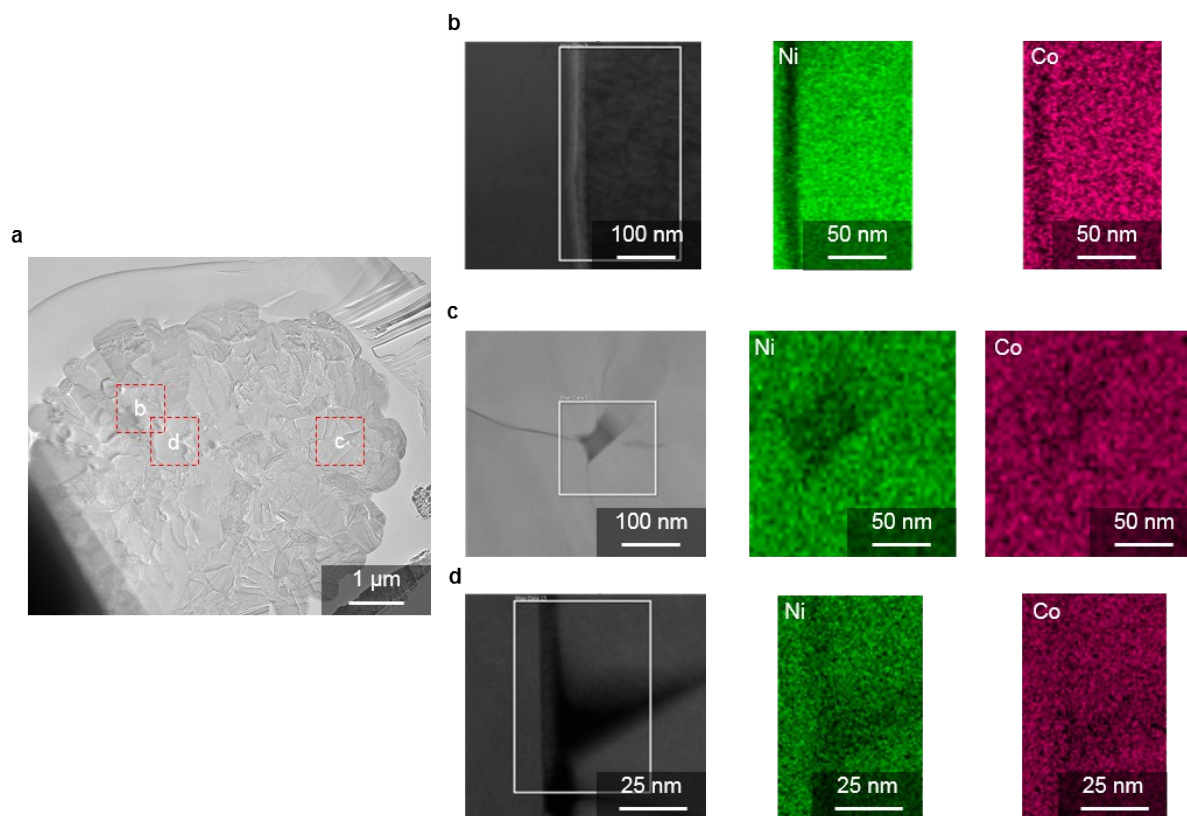


Figure S6. (a) A high resolution transmission electron microscopy (HR-TEM) image of the mixture of the NCM and stabilizer precursor after annealing at 200°C. (b-d) Scanning transmission electron microscopy (STEM) images from red boxes in (a) with their energy dispersive X-ray spectroscopy (EDX) mapping results of nickel and cobalt elements, showing interpenetration of the stabilizer precursor along grain boundary.

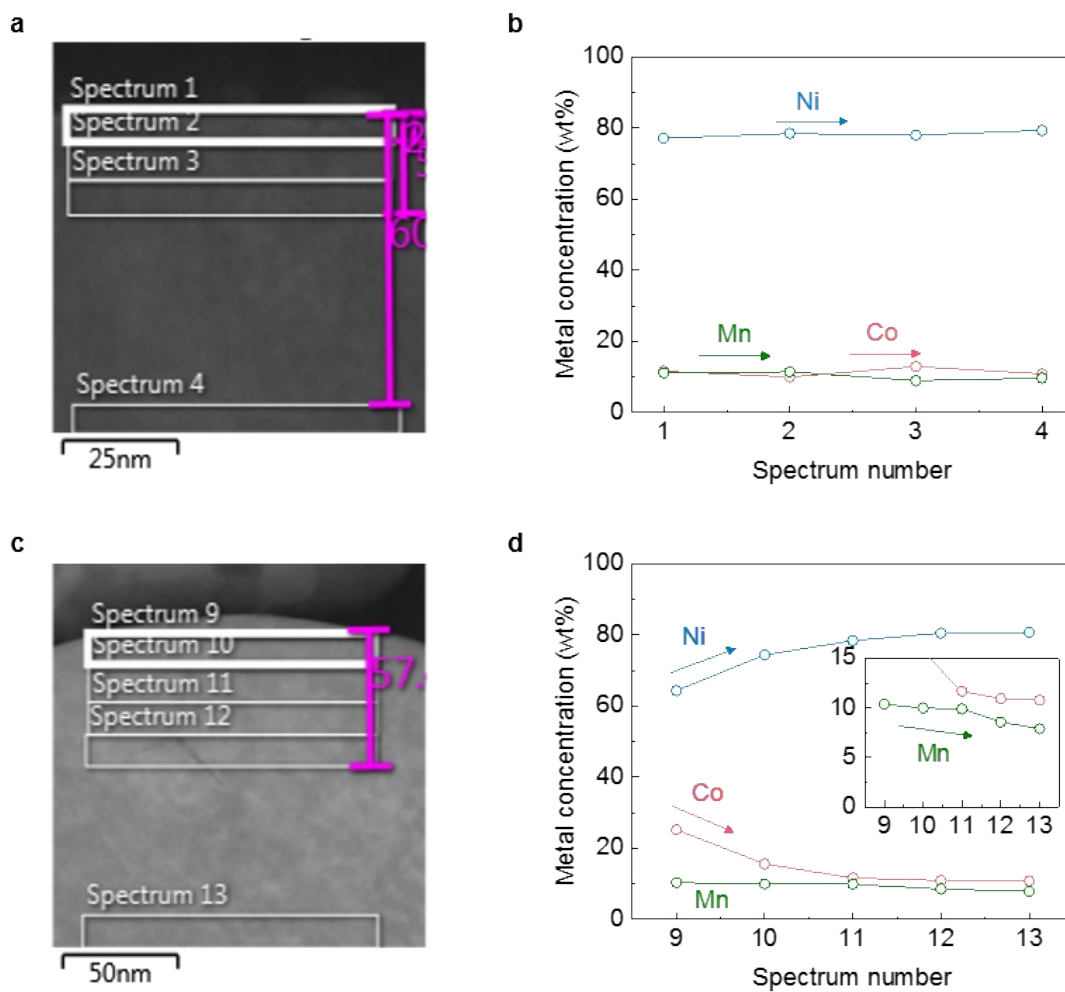


Figure S7. HAADF-STEM images of the (a) NCM and (c) NS-NCM. EDX results of the (b) NCM and (d) NS-NCM from (a) and (c), respectively.

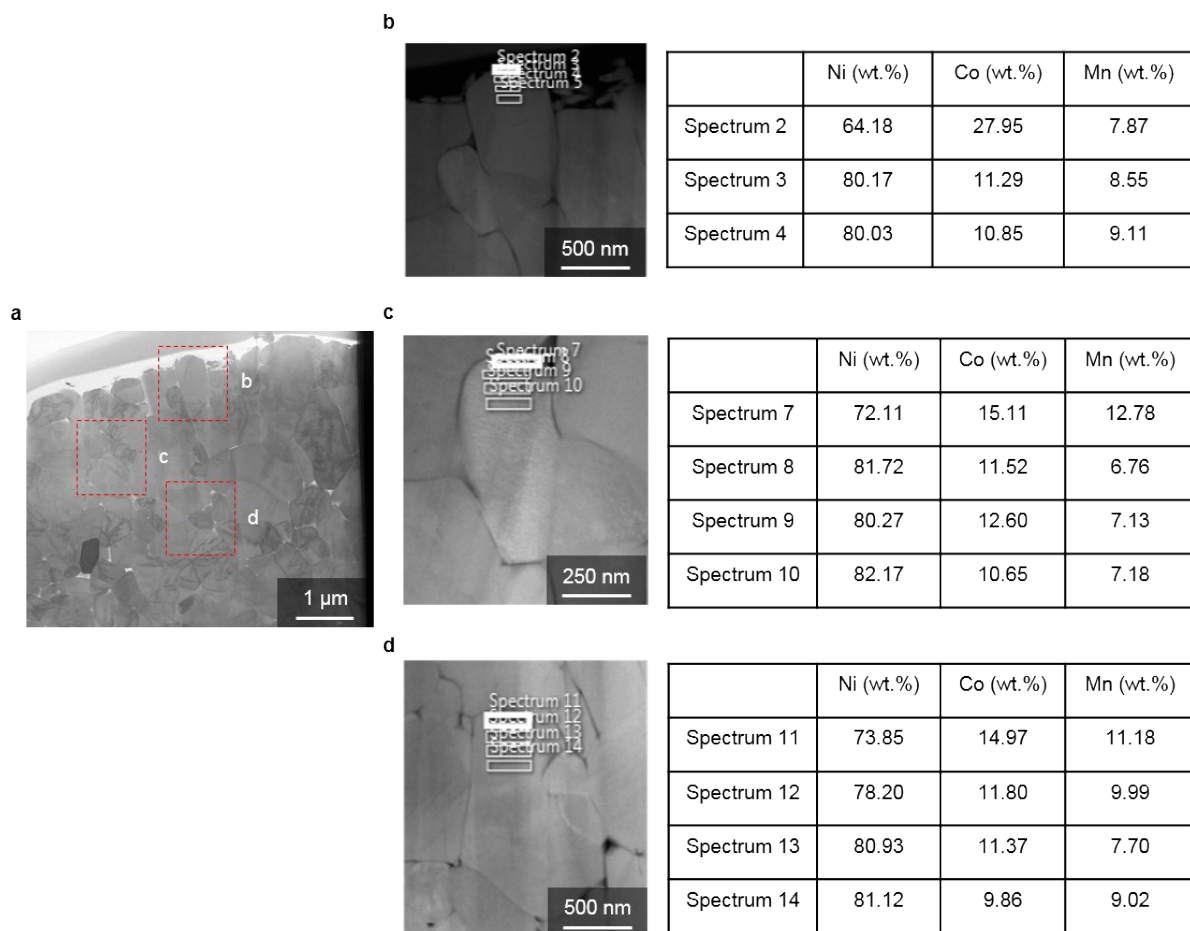


Figure S8. (a), A HAADF-STEM image of the NS-NCM. (b-d) Magnified HAADF-STEM images from (a) with their EDX results, showing the TM concentration gradient was formed throughout the NS-NCM.

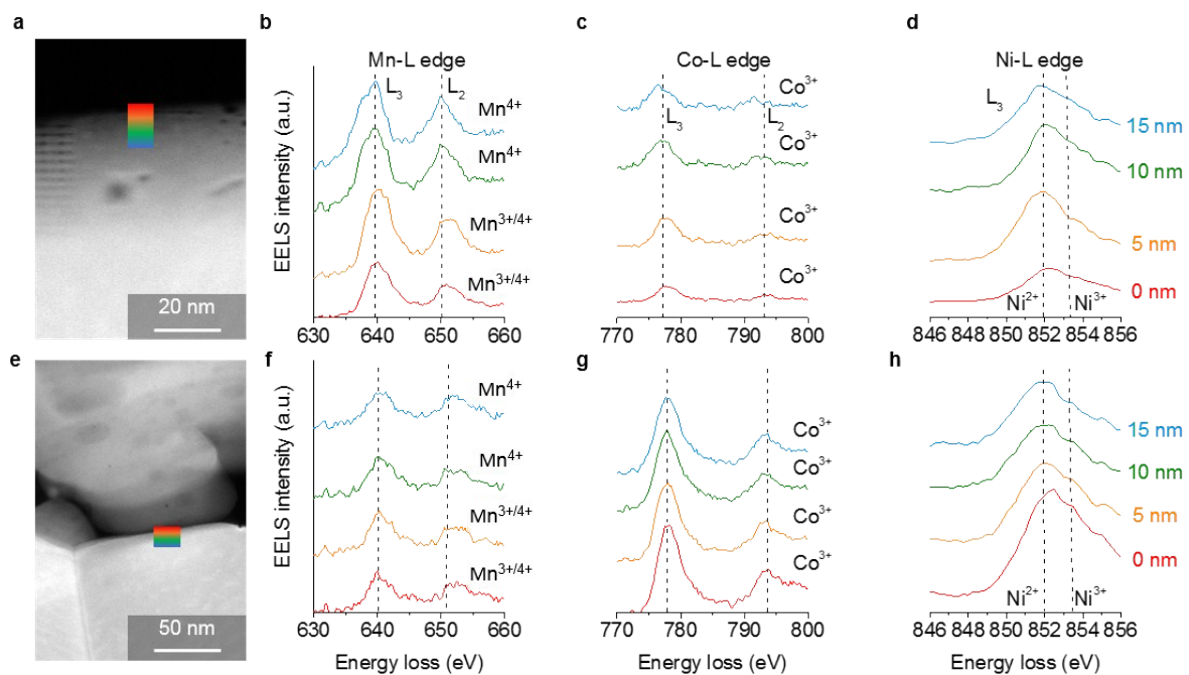


Figure S9. HAADF-STEM images of the (a) NCM and (e) NS-NCM before electrochemical test. EELS spectra of (b) Mn-L edge, (c) Co-L edge, and (d) Ni-L edge in the NCM. EELS spectra of (f) Mn-L edge, (g) Co-L edge, and (h) Ni-L edge in the NS-NCM.

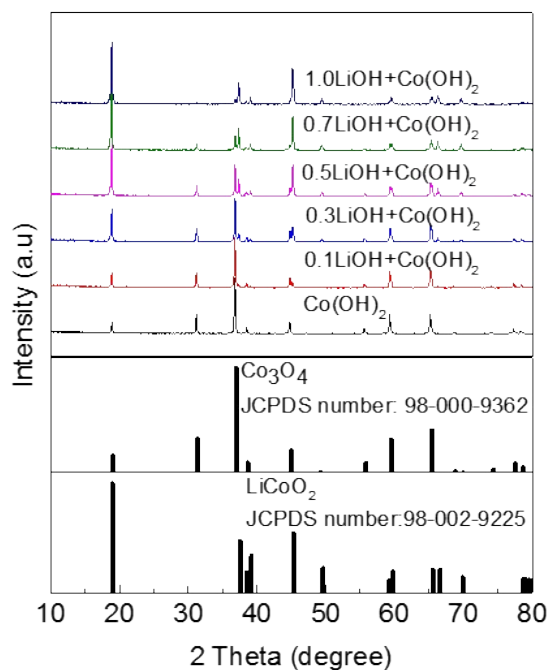


Figure S10. Powder XRD patterns after annealing the mixture of Li₂CO₃ and stabilizer precursor at 750°C under oxygen atmosphere.

To better understand the reaction mechanism between the stabilizer precursor and residual lithium compounds, we directly reacted the stabilizer precursor with the lithium carbonate as the additional lithium sources. We confirmed that the structure was gradually transformed from the Co₃O₄ spinel to lithium deficient Li_xCoO₂ (0 < x < 1) type spinel and LiCoO₂ layered structure with increasing the molar ratio of Li/Co from 0 to 1, which was confirmed by the XRD (Fig. S10, ESI†). This concept allows the NS-NCM to have the nanostructured stabilizer with epitaxially grown surface layer.

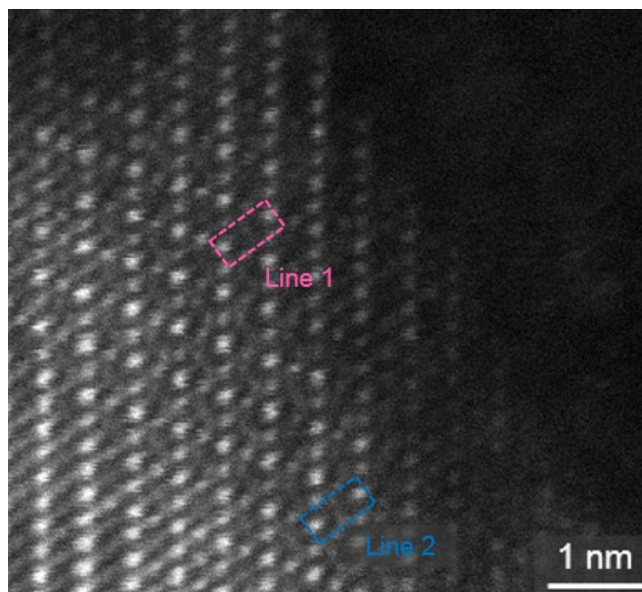


Figure S11. A magnified high angle annual dark field scanning transmission electron microscopy (HAADF-STEM) image at surface spinel region from Fig. 1g.

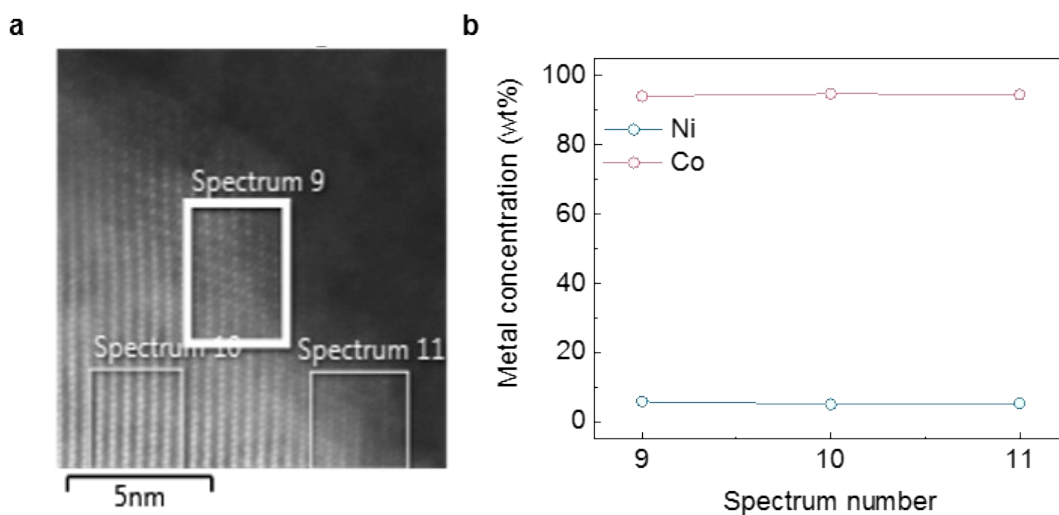


Figure S12. (a) High angle annual dark field scanning transmission electron microscopy (HAADF-STEM) image of the nanostructured stabilizer. (b) Energy dispersive X-ray spectroscopy (EDX) results from white boxes in (a).

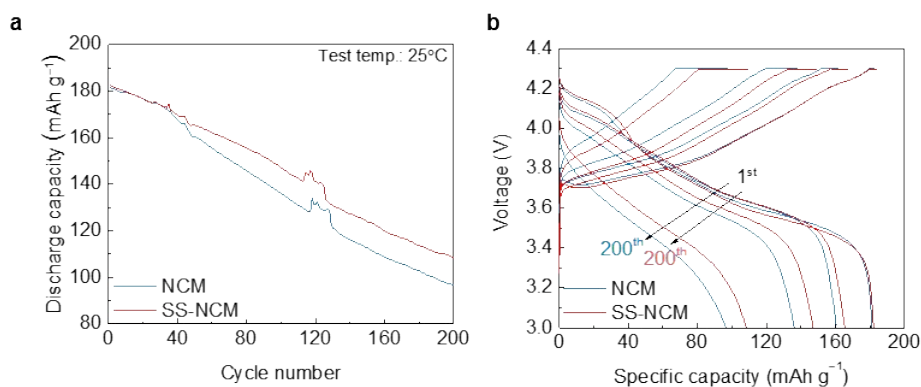


Figure S13. (a) Room temperature cycling performance of the NCM and NS-NCM in the voltage ranged from 3.0 to 4.3 V (Charge and discharge C-rate: 0.5C and 1C). (b) Voltage profiles of the NCM and NS-NCM from the room temperature cycle test at 1st, 50th, 100th, and 200th cycles.

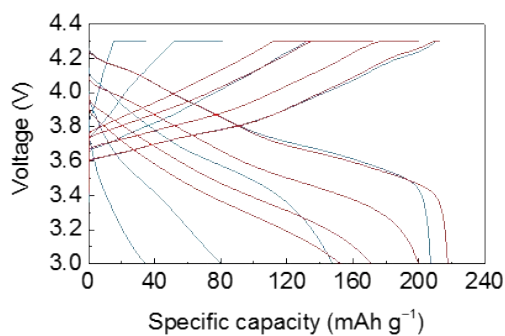


Figure S14. Voltage profiles of the NCM and NS-NCM from the high temperature cycle test at 1st, 50th, 100th, and 200th cycles (Charge and discharge C-rate: 0.5C and 1C).

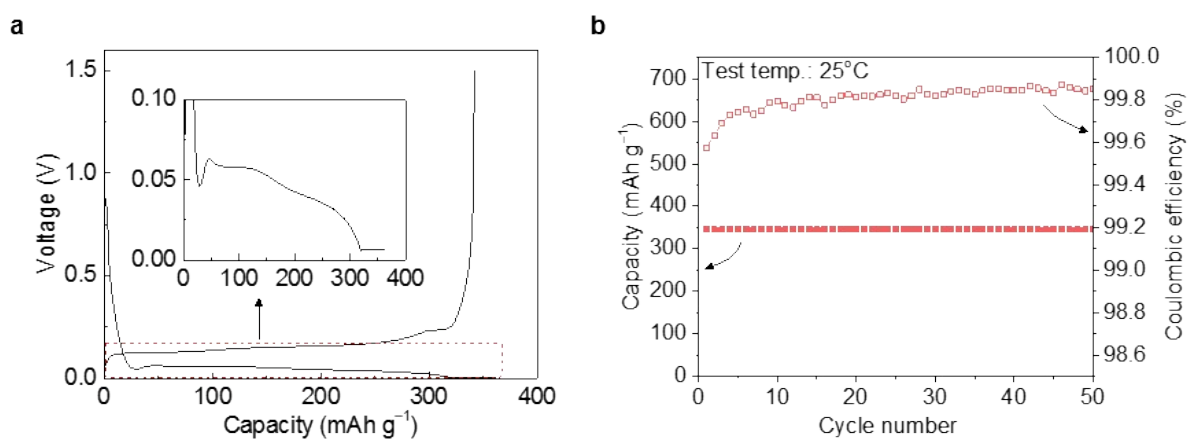


Figure S15. (a) Initial charge and discharge voltage profiles of the graphite anode in the voltage ranged from 0.0005 to 1.5 V at 25°C (both charge and discharge C-rate: 0.1C). (b) Room temperature cycling performance of the graphite anode in the voltage ranged from 0.0005 to 1.5 V (both charge and discharge C-rate:1C).

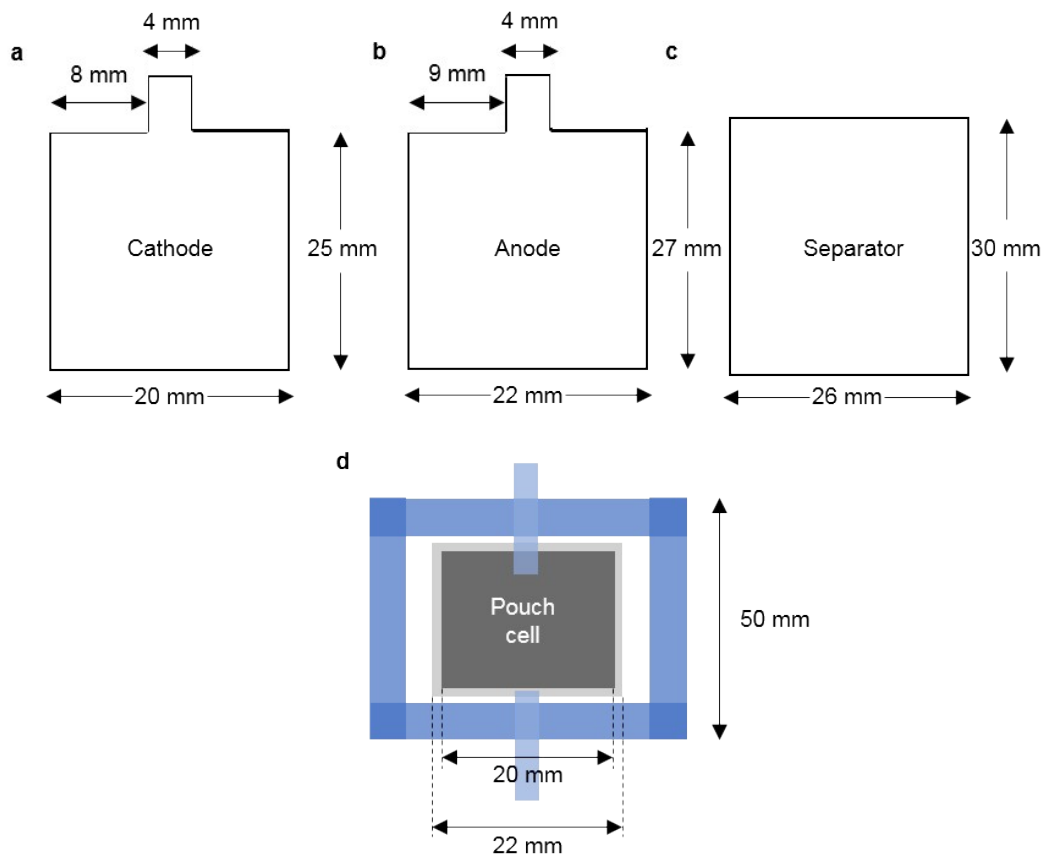


Figure S16. Size of the (a) cathode, (b) anode, (c) separator, and (d) pouch cell.

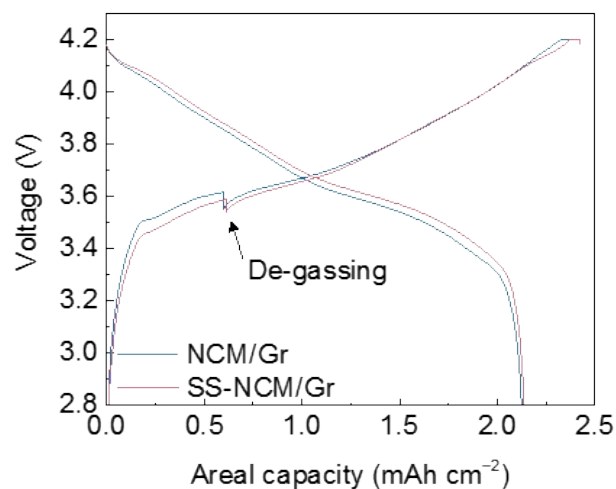


Figure S17. First cycle voltage profile of the NCM/Gr and NS-NCM/Gr full-cell in the voltage ranged from 2.8 to 4.2 V at 25°C (both charge and discharge C-rate : 0.1C). Voltage drop around ~3.6 V indicates that the self-discharge occurred in the full-cells during the de-gassing process.

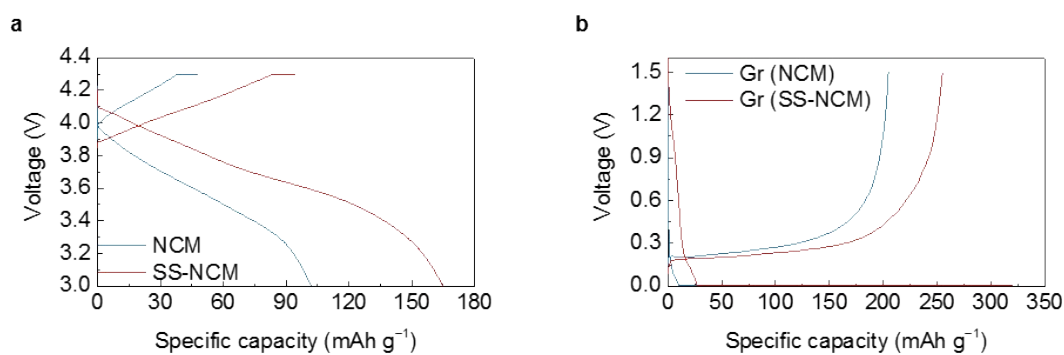


Figure S18. (a) Voltage profiles of the NCM and NS-NCM at 25°C in the voltage ranged from 3.0 to 4.3 V after reassembling the cycled cathodes in the half-cell with a fresh electrolyte and lithium metal. The cathode half-cells were charged and discharged at 0.1 C rate. (b) Voltage profiles of the graphite anode at 25°C in the voltage ranged from 0.0005 to 1.5 V after reassembling the cycled anode in the half cell with a fresh electrolyte and lithium metal. The anode half-cells were charged and discharged at 0.1 C rate.

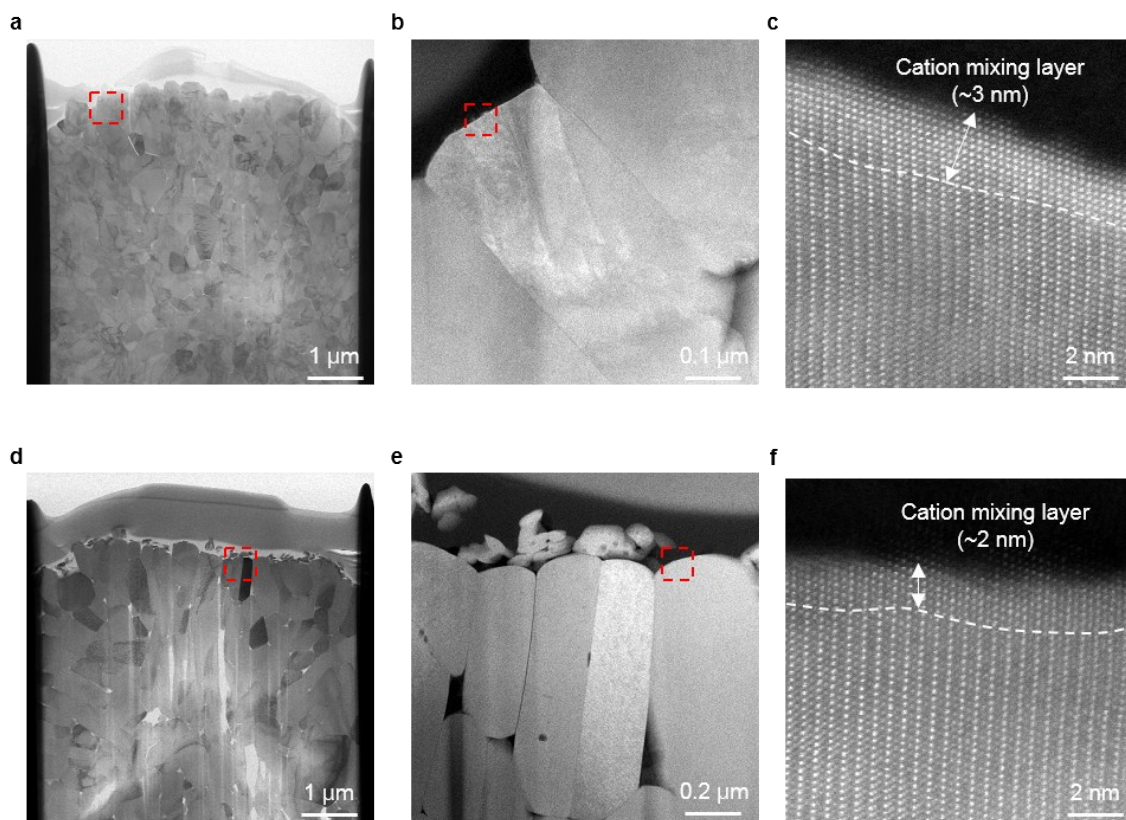


Figure S19. (a) A HAADF-STEM image of the pristine NCM. (b) A magnified HAADF-STEM image of the NCM from red box in (a). (c) A STEM image of the NCM from red box in (b). (d) A HAADF-STEM image of the pristine NS-NCM. (e) A magnified HAADF-STEM image of the NS-NCM from red box in (d). (f) STEM image of the NS-NCM from red box in (e).

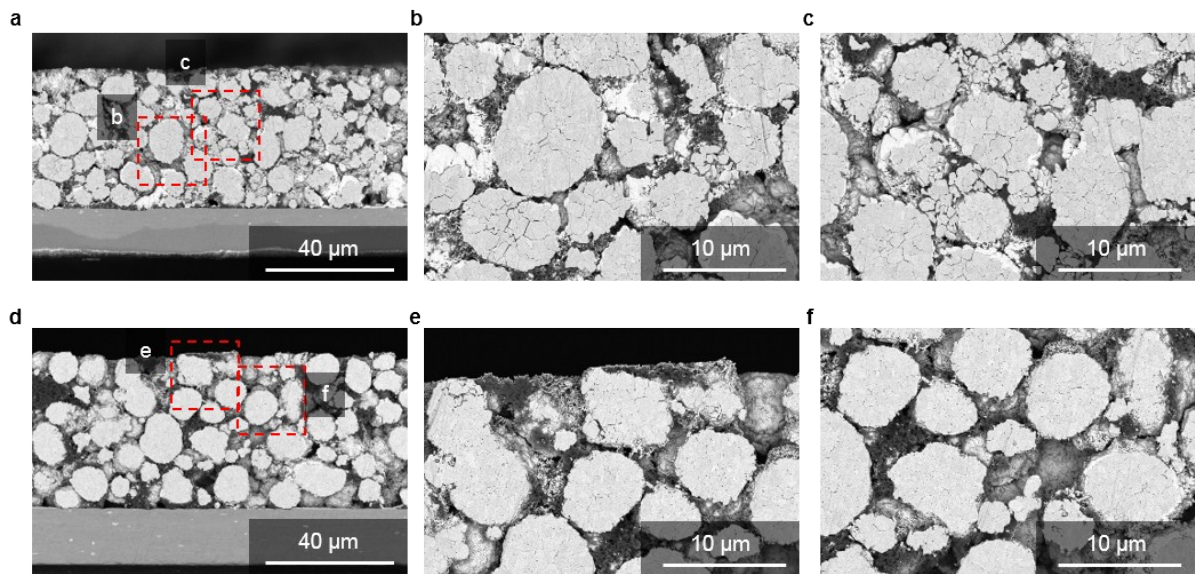


Figure S20. (a) A cross-sectional NCM electrode SEM image after 500 cycles at 45°C. (b-c) Magnified cross-sectional NCM electrode SEM images from (a) after 500 cycles at 45°C. (d) A cross-sectional NS-NCM electrode SEM image after 500 cycles at 45°C. (e-f) Magnified cross-sectional NS-NCM electrode SEM images from (d) after 500 cycles at 45°C.

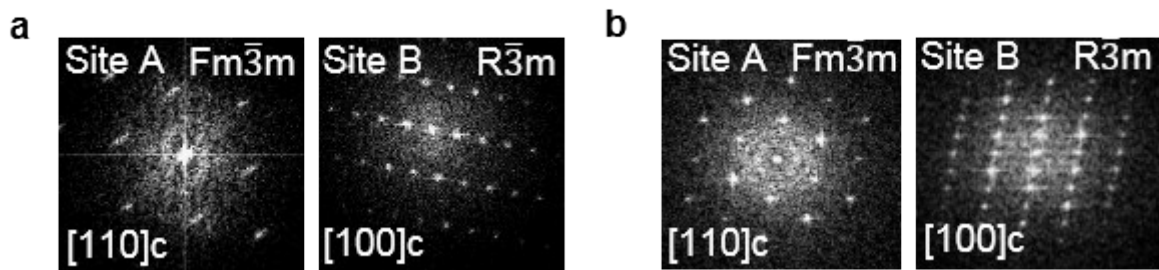


Figure S21. Fast Fourier-transform (FFT) patterns of the (a) NCM and (b) NS-NCM after 500 cycles at 45°C from the white boxes in Fig. 3b and e, respectively.

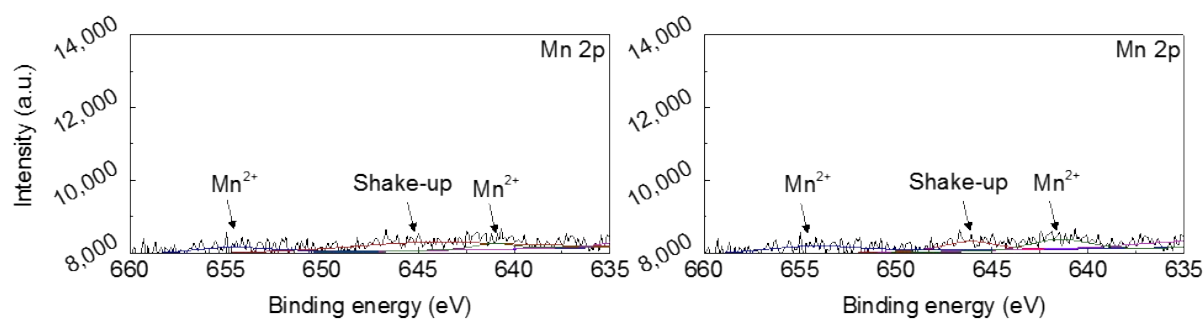


Figure S22. Mn 2p X-ray photon spectroscopy (XPS) spectra of the graphite anode in the (a) NCM/Gr full-cell and (b) NS-NCM/Gr full-cell after 500 cycles at 45°C. Shake-up peak appears because the other electrons could be excited to higher energy state by the primary photoelectrons during the photoionization process.

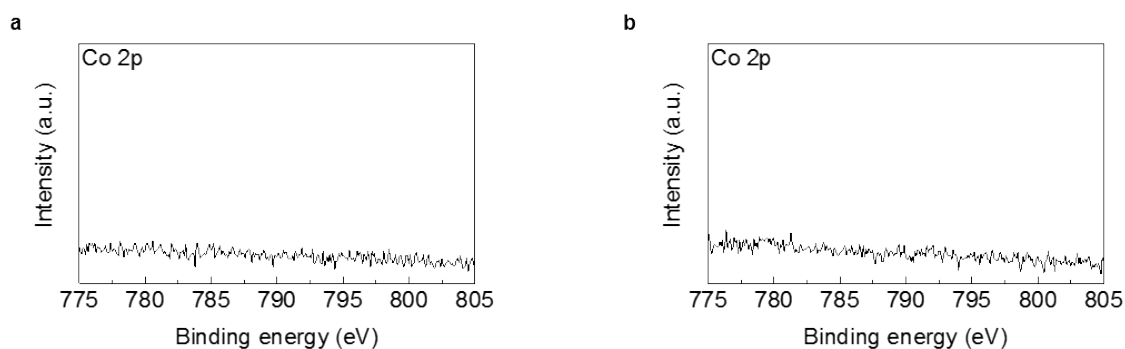


Figure S23. Co 2p XPS spectra of the graphite anode in the (a) NCM/Gr full-cell and (b) NS-NCM/Gr full-cell after 500 cycles at 45°C.

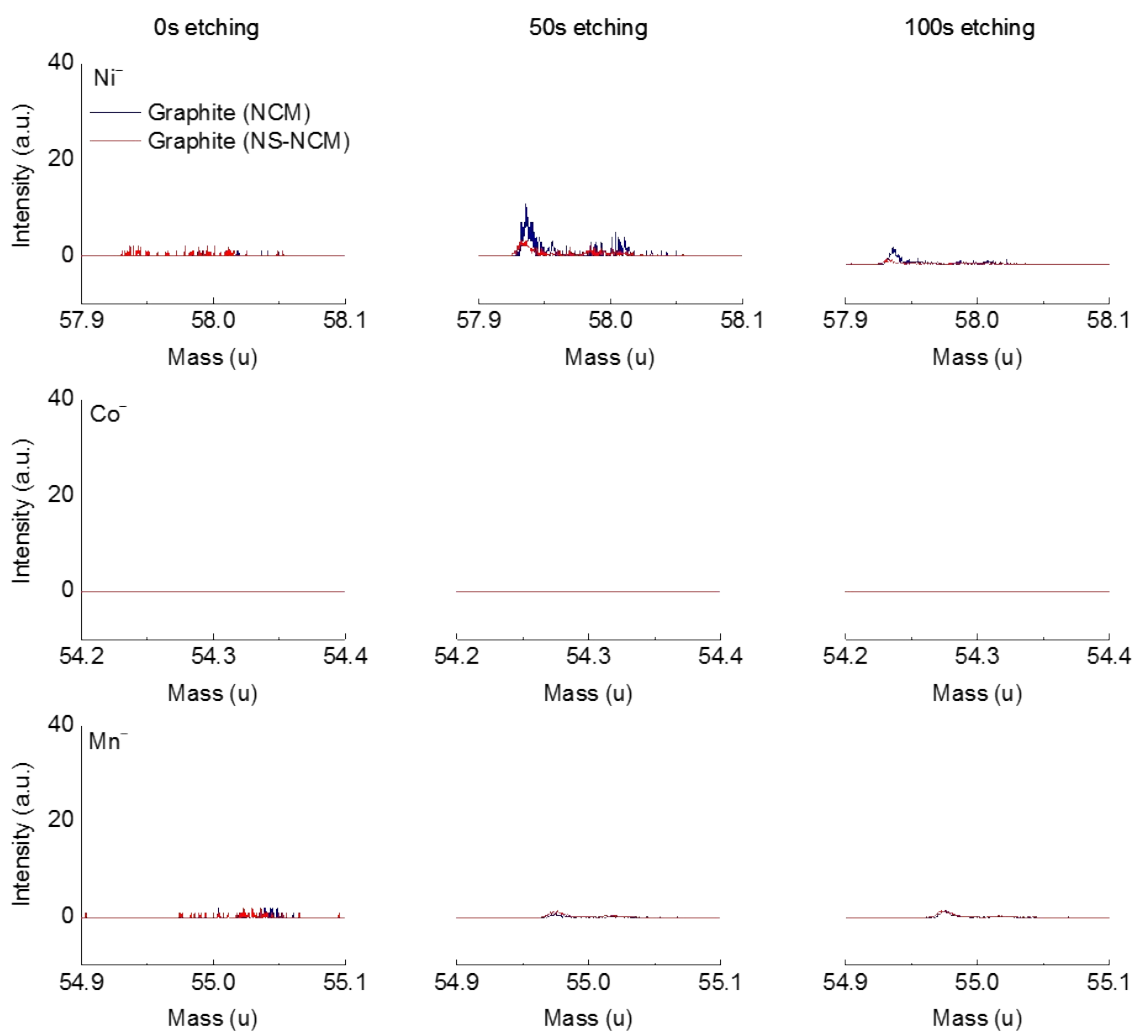


Figure S24. Time of flight – secondary ion mass spectroscopy (ToF-SIMS) results of both graphite anodes in the NCM/Gr and NS-NCM/Gr full-cell with depth profiling from 0s to 100s.

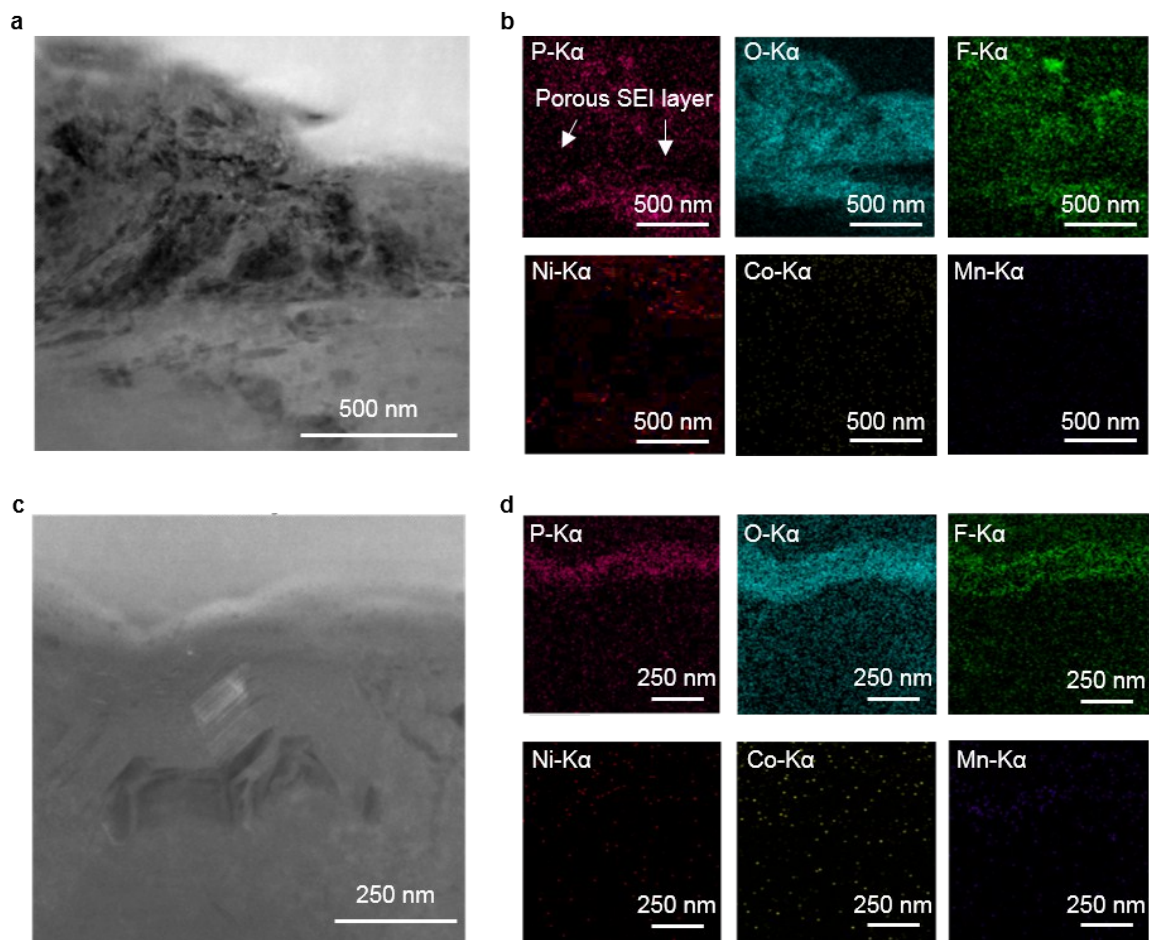


Figure S25. A magnified HAADF-STEM images of the surface of the graphite anode in the (a) NCM/Gr full-cell and (c) NS-NCM/Gr full-cell after 500 cycles at 45°C from Fig. 4e and g, respectively. EDX mapping results of the graphite anode in the (b) NCM/Gr full-cell and (d) NS-NCM/Gr full-cell from (a) and (c), respectively.

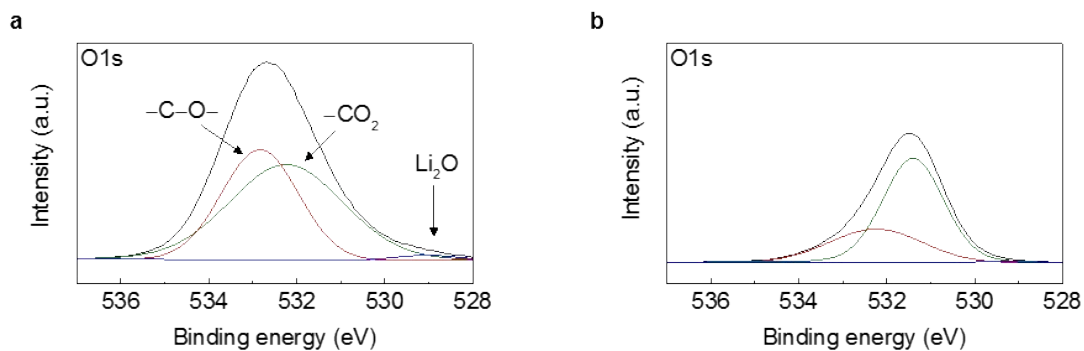


Figure S26. O 1s XPS spectra of the graphite anode in the (a) NCM/Gr full-cell and (b) NS-NCM/Gr full-cell after 500 cycles at 45°C.

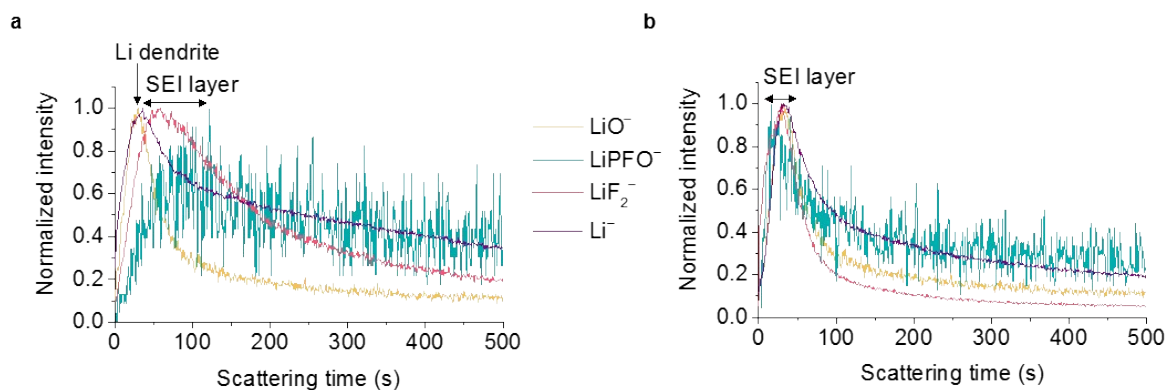


Figure S27. Time-of-flight secondary ion mass spectroscopy (ToF-SIMS) spectra of the graphite anode in the (a) NCM/Gr full-cell and (b) NS-NCM/Gr full-cell over 500 s sputtering by using Cs⁺ beam. These magnified results show lithium containing compounds collected from Fig. 5e, f.

References

1. H. Kim, M. G. Kim, H. Y. Jeong, H. Nam and J. Cho, *Nano Lett.*, 2015, **15**, 2111-2119.
2. H. Kim, S. Lee, H. Cho, J. Kim, J. Lee, S. Park, S. H. Joo, S. H. Kim, Y.-G. Cho, H.-K. Song, S. K. Kwak and J. Cho, *Adv. Mater.*, 2016, **28**, 4705-4712.
3. Y. Huang, Y. Huang and X. Hu, *Electrochim. Acta*, 2017, **231**, 294-299.
4. Y. Kim and J. Cho, *J. Electrochem. Soc.*, 2007, **154**, A495-A499.
5. M. Jeong, M. J. Lee, J. Cho and S. Lee, *Adv. Energy Mater.*, 2015, **5**, 1500440.
6. Z. Liu, H. Wang, L. Fang, J. Y. Lee and L. M. Gan, *J. Power Sources*, 2002, **104**, 101-107.
7. X. T. Chen, J. P. Tu, Y. Z. Yang, H. M. Wu and J. Y. Xiang, *Phys. Scr.*, 2007, **2007**, 49.
8. Y. Jin, Y. Xu, L. Xiong, X. Sun, L. Li and L. Li, *Solid State Ionics*, 2017, **310**, 62-70.